INSTITUTE OF PLASMA PHYSICS
CZECHOSLOVAK ACADEMY OF SCIENCES

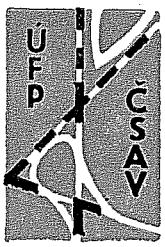

GLOBAL ENERGY BALANCE AND DENSITY LIMIT ON CASTOR TOKAMAK

Djabilin K.S.[x], Badalec J., Borschegovski A.A.[xx], Ďatlov J.,
Jakubka K., Kopecký Vl., Korotkov A.A.[xxx], Stöckel J.,
Valovič M., Žáček F.

[x] Institute of General Physics, Moscow, USSR
[xx] I.V. Kurchatov Atomic Energy Institute, Moscow, USSR
[xxx] A.F. Ioffe Physico-Technical Institute, Leningrad, USSR

RESEARCH REPORT

IPPCZ 260 December 1985

POD VODÁRENSKOU VĚŽÍ 4, 180 69 PRAGUE 8
CZECHOSLOVAKIA

ABSTRACT

Total radiative power losses have been measured by a pyroelectric detector on the CASTOR tokamak in a broad range of plasma parameters. It was shown, that while for the low density operation ($\bar{n}_e \lesssim 10^{19} m^{-3}$) the most important channel of energy losses is a thermal conductivity, the high density regimes are radiative dominant. Using a simple analytic energy balance model, the connection between such high level of radiation and shrinking of the current channel resulting in an enhanced MHD activity is discussed.

1. INTRODUCTION

The CASTOR tokamak ($R = 0.4$ m, $a = 0.085$ m, $B_T \leq 1.5$ T) is a reconstructed version of the TM-1-MH tokamak, working in the Institute of Plasma Physics, Prague, Czechoslovak Academy of Sciences. Experimental and numerical studies of the plasma energy balance on the TM-1-MH tokamak [1] have shown that:

1) in the density and current ranges $\bar{n}_e = (0.7\text{-}2.0)\times10^{19}\,m^{-3}$ and $I_p = 11 \div 17$ kA, the central electron and ion temperatures are in the range $T_e(0) = 150 \div 300$ eV and $T_i(0) = 50 \div 100$ eV respectively;
2) the energy transport through the electron channel is well described supposing the electron thermal conductivity is given by the Alcator scaling

$$\chi_e = 5\times10^{19}/n_e \qquad [m^2 s^{-1},\ m^{-3}]\ ; \qquad (1)$$

3) the dominant channel of the energy losses from the ion component is a thermal conductivity well described in terms of the neoclassical model. The charge exchange plays some role on the periphery of the plasma column, but its influence on the global ion energy balance is negligible for investigated density range.

Previous investigations performed on the CASTOR tokamak [2] have shown, that the basic plasma parameters have not changed substantially comparing to the TM-1-MH tokamak. However, for a more detailed understanding of the energy balance, it is necessary to have additional data about such important channel of the energy losses as is radiation. The radiative power losses are caused predominantly by a line radiation of impurities and

the radiation dominated discharges are hence usually characterized by a high electron density or by an enhanced concentration of impurities.

We report here an analysis of preliminary experiments devoted to investigation of the radiative power losses and the global energy balance under various discharge conditions on the CASTOR tokamak (section 2). Some local features of the electron component, especially at high density discharges, are illustrated by a simplified model of the energy balance. It's approximate solution is presented in Appendix 2. The electron density has been also increased till the stability limit and discharges with disruptions have been studied as well (section 3).

Before describing results obtained, we mention briefly the used diagnostics. The plasma current and loop voltage were monitored to determine the ohmical heating power. Line averaged electron density $\bar{n}_e$ was measured by an 4-mm interferometer. Radiative power losses P_{rad} were registered by an absolutely calibrated pyroelectric detector ($LiTaO_3$) [3], located toroidally 90^o away from the limiter. More detailed description of the detector is given in Appendix 1. An absolutely calibrated VUV monochromator (λ = 50÷610 nm) [4] was used for monitoring of different spectral line intensities. Plasma magnetohydrodynamic (MHD) activity was detected as well.

2. ENERGY BALANCE

Fig. 1 presents typical temporal evolutions of various characteristic parameters of the discharge: plasma current I_p, loop voltage U_{loop}, line average electron density $\bar{n}_e$ and radiative power P_{RAD}. All experimental results, presented below, have been obtained at the toroidal magnetic field $B_T = 1.3$ T. Plasma current I_p reaches its maximum value at about 2 ms and then it is approximately constant, as well as the loop voltage, until 6.5 ms. This quasistationary time interval has been used for the energy balance analysis. Plasma density is controlled by an impulse gas puffing. Radiative power losses are in the range of 10 kW in presented case, i.e. they are approximately 30-40 % of the OH power.

Fig. 2 shows dependence of the ohmic and radiative powers on the average density $\bar{n}_e$ at the different values of the plasma current. It may be seen, that absolute value of the radiative power doesn't depend substantially on the plasma current while it increases, in all investigated cases, approximately proportionally to the density. According to common used expression for radiative power [5] $P_{RAD} \sim \bar{n}_e^2 (Z_{eff} - 1)$ this fact indicates that the effective plasma charge Z_{eff} decreases with increasing density. It is in accordance with the spectroscopic measurements carried out in [4] as well. Consequently, for given density, the relative radiative losses P_{RAD}/P_{OH} decrease with increasing plasma current.

Because we are lacking of sufficient data about radial profiles and so we have no possibility to investigate the problem locally, our aim was to estimate the role of different energy losses channels in the global plasma energy balance only. Therefore we estimate at first the total value of power P_{ei}, transferred from electrons to the ions due to the collisions in the whole plasma volume. Fig. 3 presents an enumerated dependence of P_{ei} on the density taking into account the real dimensions of the system and assuming a priori in the whole plasma volume the electron temperature at least double the ion one. Uncertainty in the enumerated values of P_{ei} is caused by the uncertainty in the value of the ion temperature. The minimum and the maximum values of P_{ei} correspond, according our previous charge-exchange measurements, to the limit ion temperatures in the central plasma region 150 and 50 eV respectively. The absolute value of P_{ei} depends only weakly on the profiles $T_e(r)$ and $T_i(r)$. It may be seen from Fig. 3, that P_{ei} becomes a significant loss channel at sufficiently high densities of the plasma.

Comparison of the ohmic and radiative powers and the quantity P_{ei} shows that it is possible to distinguish two qualitatively different regions with respect to $\bar{n}_e$:

1) Region $\bar{n}_e \lesssim 10^{19} m^{-3}$.

The ohmic power substantially exceeds P_{RAD} and P_{ei} in this density range, what indicates that the main part of energy delivered into the plasma escapes through the electron thermal conconduction channel to the limiter (or wall). In Fig. 4 this power $P_{COND} = P_{OH} - P_{RAD} - P_{ei}$, transported through the plasma

boundary due to the thermal conduction at densities $\bar{n}_e \lesssim 10^{19} m^{-3}$, versus the plasma current I_p is presented. By dotted line the same power, but computed according formula

$$P^*_{COND} = \frac{3}{2} \frac{\langle n_e T_e \rangle V}{\tau_{Ee}}$$

is given. For this computation the average electron temperature was estimated according to the Spitzer conductivity formula taking $Z_{eff} = 2$. Here V denotes plasma volume, τ_{Ee} the electron energy confinement time connected with the losses due to the thermal conductivity $\tau_{Ee} = a^2/4\chi_e$, where $\chi_e = 2.5 \times 10^{19}/\bar{n}_e$ $[m^2 s^{-1}, m^{-3}]$. The value of the constant in χ_e was choosen to ensure the best fitting of P^*_{COND} with the curve P_{COND}. This value is one half of that in the Alcator scaling (see eq. (1)). In spite of somewhat rough estimation the difference is not so great. Finally, it is interesting to note, that in this density range the quantity P_{COND} is for given current practically independent on $\bar{n}_e$ (see also Fig. 5). It indicates, that χ_e is really inversely proportional to the $\bar{n}_e$, as Alcator scaling predicts.

2) Region $\bar{n}_e \gtrsim 10^{19} m^{-3}$.

In Fig. 5 the dependences of the input ohmic power, power transferred from electrons to the ions, radiative power and quantity $P_{COND} = P_{OH} - P_{RAD} - P_{ei}$ are given for different values of the plasma current. While for densities $\bar{n}_e \lesssim 10^{19} m^{-3}$ the main part of the plasma energy escapes through the plasma boundary due to the thermal conductivity, for densities $\bar{n}_e > 10^{19} m^{-3}$ the influence of this channel upon the energy balance is significantly weaker. The decrease of P_{COND} could be a

consequence of the flattening of the electron temperature profil at the column periphery, maybe connected just with an enhancemen of the radiative losses and transport of heat from electrons to the ions in this region. Indeed, in this range of $\bar{n}_e$, the effect of mechanisms mentioned would be quite decisive as the total power lost by radiation represents more than one half of the ohmic one (see Fig. 5) and the power transferred to the ions has been already approached value about 10-20 % of the input power at $\bar{n}_e \simeq 2.5 \times 10^{19} m^{-3}$. If the density increases up to $\bar{n}_e \gtrsim 2.5 \times 10^{19} m^{-3}$ the effect of the thermal conduction becomes quite negligible. The global energy balance of the plasma is then determined by the radiation and energy transfer to the ions only. At densities $\bar{n}_e \simeq 3 \times 10^{19} m^{-3}$ the contribution of these two channels are comparable and each of them equals approximately one half of the ohmic power for $I_p = 17$ kA.

The investigation of the energy balance at still higher densities is more questionable. Brief comparison of the established power losses with ohmical input (Figs. 2 and 3) shows, that even neglecting conductivity losses, we obtain a discrepancy in the quasistationary power balance: $P_{ei} + P_{RAD} > P_{OH}$. One possible explanation of this discrepancy could be connected with charge-exchange power losses P_{ex} [x]. This loss channel is included in the term P_{ei} but, on the other hand, the charge-exchange atoms are registered by the pyroelectric detector, i.e. they enter the

---

[x] An other uncertainty in the energy balance follows from a certain non-stationarity of $\bar{n}_e$ at the sufficiently great gas puffin However, a simple estimation of the term $\partial W_e/\partial t = \partial(\bar{n}_e \bar{T}_e)/\partial t$ shows, that this effect is not substantial.

P_{RAD} as well. Therefore, if the charge-exchange atoms play a significant role in the global energy balance, the real radiative losses would be correspondingly lower than the raw output data from the bolometer. To solve this problem, the signal from bolometer was compared with the time evolution of intensity of the spectral line O VI (λ = 103 nm) which should be representative line from the point of view of the energy balance in high current and density discharges [4]. Concordance of the both evolutions (see Fig. 6) suggests, that comparing with the line radiation the effect of the charge-exchange loss channel is negligible even at the highest densities. There are only differencies at the start-up ($t \lesssim 1.5$ ms) and final ($t \gtrsim 8$ ms) phases of the discharge, when radiation losses are probably attributed mainly to ions with lower degree of ionization. From the suggestion, that the radiation power P_{RAD} is measured by the pyroelectric detector correctly one can conclude, that the condition $P_{ei} = P_{OH} - P_{RAD}$ has to be fulfilled. Fig. 7 presents the energy balance for densities $\bar{n}_e \gtrsim 2.5 \times 10^{19} m^{-3}$ evaluated under this condition (i.e. $P_{ex} \simeq 0$, $P_{COND} \simeq 0$). The observed decrease of the power transferred from electrons to ions P_{ei} with density indicates an equilibrisation of the temperatures of the both components.

As it was already emphased above, we have not possibility to investigate the energy balance of electron component locally. Nevertheless, to understand and to demonstrate some local phenomena in more details, especially at high densities, a simplified model of the energy balance of electrons is discussed in Appen-

dix 2. The model, assuming that the ohmical power is dissipated mainly in the central region of plasma column and energy is transported to the periphery by the thermal conductivity, where it is then lost by impurities ions radiation, is developed on the basis of the available experimental data (the corresponding balance equation see eq.(A1)). An approximate analytic solution outlined in Appendix 2 permits us to estimate a "characteristic width Δ" of the electron temperature radial profile (supposing $T_e \sim \exp(-x^2/\Delta^2)$) as a function of ratio β of the total radiated and ohmical powers $\beta = P_{RAD}/P_{OH}$. Fig. 8 illustrates the contraction of the electron temperature profile with increasing β. Qualitatively similar results have been obtained by a numerical calculation of the energy balance in papers [5,6].

The peaking of the electron temperature is consequently followed by a current channel shrinking. Some experimental aspects of this phenomenon (existence of a density limit, disruptive instability etc.) on CASTOR tokamak are discussed in the next chapter.

3. CRITICAL DENSITY

It is well known, that increase of the plasma density in tokamak above some limit results in the instability [7]. In this paragraph we discuss the results of preliminary investigation of such high density regimes, in which the discharge becomes unstable.

Fig. 9 presents the time evolutions of the toroidal current, loop voltage, radiative losses and plasma MHD activity during the discharge with a disruptive instability at time $t = 5.7$ ms. As the toroidal current changes only slightly during the instability, we can characterize this instability like "minor" one according Kadomtsev classification [8]. It may be seen, that while the radiative losses follow the plasma density increase until the disruption (in the same way as during the stable discharge), they increase suddenly in the moment of instability. In contrast to the MHD activity, no precursor before the negative spike of the loop voltage is observed. Simultaneous small increase of the toroidal current and negative loop voltage spike indicate fast decrease of the plasma column inductance (fast inward motion of the current channel and maybe its expansion as well). Moreover, after the disruption the hard X-ray radiation (HXR) observed during the discharge (not shown in Fig. 9) disappears. It indicates an escape of high energy electrons from the plasma.

To show the operating region of the CASTOR tokamak, we present the stability diagram [7] in Fig. 10. The hatched area corresponds to the unstable discharges. The quantity $\bar{n}_{cr}$ is a critical density above which the discharge becomes unstable. The parameter $\bar{n}_{cr} \cdot R/B_T$ is related to the relative level of radiation $\beta = P_{RAD}/P_{OH}$, as it has been shown in [6].

Fig. 11 shows oscillograms of signals from the four magnetic probes, uniformly distributed around the liner in a poloidal cross-section and registering the disturbance $\tilde{B}_\varphi$ of the polo-

ldal magnetic field B_φ . It may be seen quite regular oscillations corresponding to the m = 2 mode before disruption.

In Fig. 12 the temporal dependence of the ratio $\tilde{B}_\varphi / B_\varphi$, frequency of the oscillations for corresponding mode number f/m and the island width δ estimated as $\delta = b\sqrt{\tilde{B}_\varphi / B_\varphi}$ [9] are given. By b the radius of magnetic coil position is denoted. The island width δ evaluated in such way increases rapidly approaching the disruption and its maximum value reaches 3-4 mm. Simultaneously frequency of the iscillations decreases. The increase of δ may be connected with a sharpening of the current density profile. In Fig. 13 a calculated dependence of the island width for mode n = 2 on the parameter α, assuming the current profile j(r) in the form $j(r) = j(0)\left[1 - (r^2/a^2)\right]^\alpha$, is given. The calculation was carried out on the basis of the quasilinear theory [10] x). The value of the safety factor on the plasma boundary was taken 6.5 in this calculation (i.e. I_p = 17 kA).

As we can see from Fig. 13, the resonant point is shifted from the plasma center to the periphery with sharpening of the j(r) profile. Simultaneously the island width grows and achieves the value about 3-4 mm. Note, that the value of island width for m = 3, n = 2 is substantially smaller and so decisive contribution to the MHD activity gives mode m = 2, n = 1 only. It follows from calculations that the maximum value of the δ in this mode is reached at the sufficiently sharp current profile. Such profile sharpening could be caused by a high level of radiative

x) More detailed description of the simulation for CASTOR tokamak is presented in [5].

osses (see Appendix 2). The strong profile sharpening could ven result in the appearance of the m = 1 mode in the central lasma region. The simultaneous existence of two modes m = 1 nd m = 2 could lead to a minor disruption. An analysis of sig- als from the magnetic probes shows, that in the moment of dis- uption the oscillations of mode m = 2 are transformed into the scillations with a higher frequency (see Fig. 9), which may be onnected just with m = 1 mode existence.

. CONCLUSION

The total radiative power P_{RAD} has been measured in a broad ange of plasma parameters on the CASTOR tokamak. It has been ound that the radiative power losses P_{RAD}:

(i) are practically independent on the plasma current;

ii) they increase proportionally to the plasma density.

he only linear increase of P_{RAD} with density indicates some dec- ease of the effec.ive charge Z_{eff} (it has been supported by spe- troscopic measurements). Moreover, measuring the ohmical input P_{OH} and estimating the power transferred to ions P_{ei} simultane- ously, we were able to estimate the power losses by the thermal conductivity P_{COND} of the electron component and, in some sence, o establish a global energy balance of this component. It has been found that at the low density regimes ($\bar{n}_e \leq 10^{19} m^{-3}$) the conductivity channel is comparable with the ohmic input, while he high density discharges with $\bar{n}_e \geq 3 \times 10^{19} m^{-3}$ can be considered s radiative dominant. Decrease of the conductivity losses with

.ncreasing density can lead to an increase of the plasma-limiter .nteraction (improvement of thermoisolation of the plasma column) ınd consequently to a decrease of an impurities influx (and con- ;equently a decrease of Z_{eff}) as it is indicated by the experiment.

The relatively high level of the radiative power losses at ıigh density should have an influence on the local parameters)f the plasma as well. A simple analytic model of the energy)alance has demonstrated a contraction of the radial electron temperature profile caused by increasing ratio $\beta = P_{RAD}/P_{OH}$. Some experimental aspects of this effect are reported. Because the electron temperature radial profile is connected with a radial distribution of the toroidal current, we have observed at high density regimes phenomena caused by a shrinking of the current channel as enhancement of the MHD activity, followed by disruptive instabilities. Simultaneous experimental and numerical studies of a disruptive discharge with relatively high $q(a) \doteq 6.5$ have shown, that the observed MHD activity is possible to inter-)ret as a formation of a magnetic island m = 2 with the width reaching the value 3-4 mm just before the minor disruption. The corresponding calculated radius of the resonant surface $r_s = a/2$ implies a model current distribution $j = j(0)(1 - r^2/a^2)^{\alpha}$ for $\alpha = 5-6$. However, the resonant surface m = 1 is appearing in the central region of the plasma column for such rather con- ;racted current profile. Simultaneous existence of the both mentioned modes can lead to the minor disruption under our conditions.

From experimental data (see Fig. 12) it is possible to estimate a rotational velocity of the magnetic island m = 2 as $v_\varphi(r_s) = 2\pi . r_s . f/m \doteq 2.5 \times 10^3$ m/s just before the disruption. Supposing v_φ to be connected with the existence of a radial electric field E_r and the toroidal magnetic field B_T, we can estimate $E_r = v_\varphi . B_T \cong 3 \times 10^3$ V/m. On the other hand, the observed value of v_φ well agrees with the velocity of a diamagnetic plasma rotation at the radius $r = r_s = a/2$:

$$v_{diamag} = \frac{\nabla p / r = r_s}{n_e(r_s) . e . B_T} \simeq \frac{2\, T_e(0)}{a . B_T} \quad [m s^{-1}, m, eV, T]$$

for $T_e(0) \cong 150$ eV ($p = n_e . T_e$ is the plasma kinetic pressure).

APPENDIX 1

Pyroelectric detector.

The pyroelectric effect is connected with a change of the spontaneous polarization P_s of a convenient pyroelectric material, due to a change of its temperature. The current generated is given by the expression:

$$I = A \cdot \frac{dP_s}{dt} = A \cdot \frac{\partial P_s}{\partial T} \cdot \frac{\partial T}{\partial t} = \frac{\partial P_s}{\partial T} \cdot \frac{P}{\ell \cdot \rho \cdot c} = f \cdot P,$$

where P_s - the spontaneous polarization per unit area of the detector,

A - area of the detector,

ρ and c - the mass density and specific thermal capacity of the detector material respectively,

P - power absorbed by the detector.

For the crystal $LiTaO_3$ used as a pyroelectric detector, the quantity $\partial P_s/\partial T$ depends only weakly on the temperature for $T \leq 400^{\circ}C$. Moreover, it was experimentally proved, that sensitivity of this detector is practically constant in a very broad range of photon energy. For samples used in the experimant reported here the quantity $\partial P_s/\partial T$ has been determined by absolute calibration of the detector using a synchrotron radiation with a known intensity and spectrum corresponding well to the distribution of line radiation of the hot plasma ($\lambda \leq 100$ nm) [3]. Bellow, the basic parameters and dimensions of the detector used are summarized:

$$f \equiv \frac{\partial P_s}{\partial T}(30^{\circ}C) = 1.2 \times 10^{-4}\ C/m^2K\ ;\ \rho = 7.45 \times 10^{3}\ kg/m^3\ ;\ c = 460\ J/kg\,K\ ;$$

ℓ = 0.5 mm, diamater 10 mm, A = 49.35 mm^2. These data give us the following absolute sensitivity of the detector:

$$\mu \equiv \frac{\partial P_s}{\partial T} \cdot \frac{1}{\ell \cdot \rho \cdot c} = 7 \times 10^{-8} \text{ A/W} .$$

The equivalent circuit of the detector and measuring circuit are depicted in the Fig. A1. Here R_D, C_D are internal resistance and capacity of the detector and R, C are the constant of the measuring circuit. As usually $R_D \gg R$ ($R_D \simeq 10$ GΩ while $R \leq 1$ MΩ), we have the following time resolution of the detector:

$$\tau = R (C + C_D) .$$

For our conditions it is desirable to have $\tau < 100$ μs and at given capacity $(C + C_D) \simeq 800$ pF we have used the value of measuring resistance R = 0.1 MΩ.

The detector is mounted on the movable support, so that the position of the detector with respect to the plasma column can be changed.

Finally, we will discuss the calculation of the total radiated power P_{RAD} from the toroidal plasma column on the basis of the experimental data obtained by means of the described pyroelectric detector. Under assumption of the uniform distribution of the radiated power over the whole inner surface of the liner, for the crystal located at the liner radius, the power registered by it P_D is

$$P_D = \frac{A^*}{S_\ell} P_{RAD} ,$$

where A^* is the active area of the detector and $S_\ell = 4\pi^2 R a$ is the area of the liner. The last expression allows to determine the quantity P_{RAD}.

It is necessary to note, that in addition to the radiation the detector is sensitive to the flux of charge-exchange neutrals as well. It is not possible, in principle, to distinguish the contributions of these two effects. Charge-exchange atoms can play significant role in discharges with a relatively high density and ion temperature namely.

APPENDIX 2

A simple analytic model of the electron component energy balance of the plasma in a high density tokamak regime.

In the following analysis we suppose, that the power is radiated from the periphery and that this radiated power loss is substantially less than the ohmic heating power in the central region. We suppose further, that the energy transfer from electrons to ions is also many times less than the ohmic heating power and doesn't influence substantially the balance of electron energy. Both supposions are usually fulfilled in tokamak experiments.

We start from the stationary balance equation:

$$-r^{-1}(r n_e K_{ek} T_e')' = P_{OH} - P_{RAD} \,, \qquad \text{(A1)}$$

where r is radius, $(\ )' \equiv \frac{\partial}{\partial r}$, K_e is heat conductivity of electrons, P_{OH}, P_{RAD} is ohmic and radiative power density, respectively. Supposing $K_e = \beta / n_e$ (β = const), $T_e = T_e^0 \Theta(r)$ ($T_e^0 \equiv T_e(0)$) and denoting $x = r/a$ (a is the plasma radius), $k = 1.6 \times 10^{-19}$ J/eV,

the eq. (A1) becomes:

$$-x^{-1}(x\theta')' = p^*_{OH} - p^*_{RAD} \quad . \qquad (A1')$$

Here $(\ )' \equiv \frac{\partial}{\partial x}$ and $p^* = p \cdot \frac{a^2}{k_f T_e^0}$.

If the influence of trapped electrons on the conductivity is neglected, the ohmic heating power density p_{OH} and normalized expression p^*_{OH} equal:

$$p_{OH} = \sigma E^2 = \frac{\alpha T_e^{0\,3/2}}{Z_{eff}} E^2 \theta^{3/2} \qquad [W/m^3,\ eV,\ V/m] ,$$

$$p^*_{OH} = \frac{a^2 \alpha \sqrt{T_e^0}}{k_f Z_{eff}} E^2 \theta^{3/2} .$$

Here σ is the Spitzer plasma conductance ($\alpha = 1.5 \times 10^3$ and Z_{eff} is effective charge of the plasma), E is a toroidal electric field. In the following we suppose the function $\theta(x)$ in the form $\theta(x) = \exp(-x^2/\Delta^2)$, where the parameter Δ determines the width of the radial T_e profile. If we put such form of $\theta(x)$ into eq. (A1'), supposing in the central region $x \ll \Delta$ validity of inequality $p^*_{RAD} \ll p^*_{OH}$, we can obtain easily the central value of $p_{OH}(0)$ as a limit expression:

$$p^*_{OH}(0) = \lim_{x \to 0} p^*_{OH} = \frac{4}{\Delta^2} .$$

The central electron temperature is then following:

$$T_e^0 = \left[\frac{I_p \sqrt{Z_{eff}}}{\sqrt{\alpha k_f}\ \pi a \Delta C} \right]^{4/5} , \qquad (A2)$$

where I_p is the total plasma current $I_p = \int_0^a \sigma E\, 2\pi r dr$

and constant C equals:

$$C = \frac{4}{3}\left(1 - e^{-\frac{3}{2\Delta^2}}\right) = 1.27 \pm 0.07 \quad \text{for} \quad \Delta \in \langle 0;\ 0.8 \rangle .$$

The toroidal electric field E, assuming to be independent on the radius, can be expressed as follows:

$$E = \left[\frac{32\,\pi (k\gamma)^3\, C\, Z_{eff}^2}{\alpha^2 a^4 \Delta^4 I_p} \right]^{1/5} . \qquad (A3)$$

For the determination of the influence of radiation on the plasma parameters, we use eq. (A1′) in an integral form:

$$-x\,\Theta'(x)\Big/_{x=x_0} = \int_0^{x_0} (p^*_{OH} - p^*_{RAD})\, x \cdot dx \; . \qquad (A1'')$$

Behaviour of the function $-x\Theta'/_{x_0}$ (quantity proportional to the heat flow through the surface with normalized radius $x = x_0$) and normalized ohmic power dissipated inside the volume with radius $x = x_0$ $P^*_{OH}(x_0) = \int_0^{x_0} p^*_{OH}(x)\, x.dx$ is shown in Fig. A2, respectively. The expression for the total normalized ohmic heating power, dissipated in the whole cross-section per unit length of the plasma column, we can derived under knowledge of the central value of $p^*_{OH}(0)$ given above:

$$P^*_{OH} = \int_0^1 p^*_{OH}(x)\, x \cdot dx = \int_0^1 \frac{4}{\Delta^2}\, \Theta^{3/2}(x)\, x \cdot dx = C \; .$$

Value of the constant C see above. On the other hand, the normalized heat flow $x\Theta'$ across the plasma boundary equals:

$$x\Theta'\Big/_{x=1} = \frac{2}{\Delta^2}\, e^{-1/\Delta^2} \; .$$

The fact, that $x\Theta'/_{x=1} < P^*_{OH} = C$, is connected with the presence of the radiative losses. The relative value of these losses $\beta = P^*_{RAD}/P^*_{OH} = P_{RAD}/P_{OH} < 1$ is therefore simply related to the characteristic width of the temperature profile Δ :

$$\beta = 1 - \frac{2}{C}\,\frac{e^{-1/\Delta^2}}{\Delta^2} \; . \qquad (A4)$$

The last relation (A4) is possible to find depicted in Fig. 8 (sec. 2) of this preprint. According to that figure the radial profile $T_e(r)$ can be substantially influenced by the presence of strong radiation. Raising the radiative loss from 40 to 100 % reduces its characteristic width from 0.8 to 0.4, i.e. to the one half.

The level of radiation impairs the energy confinement time τ_{Ee} of the electron component as well. Employing the previously obtained approximations we can write:

$$\tau_{Ee} = \frac{W_e}{P_{OH}} = \frac{W_e}{I_p \cdot 2\pi R E} = \frac{27}{32} \frac{\bar{n}_e a^2}{\mu} \cdot \frac{\Delta^2\left[1+\Delta^2\left(e^{-1/\Delta^2}-1\right)\right]}{\left(1-e^{-3/2\Delta^2}\right)} \quad \text{(A5)}$$

Here $W_e = \frac{3}{2}\int_0^a n_e T_e 2\pi R 2\pi r dr$ is the total energy of the electron component. In estimate the parabolic profile of the electron density was used (line averaged density $\bar{n}_e = \frac{2}{3} n_e(0)$). Using the eq. (A4), we can get dependence τ_{Ee} on β. In Fig. A3 the dependence of τ_{Ee}^{Norm}, the normalized energy confinement time, on β is given:

$$\tau_{Ee}^{Norm} = \tau_{Ee}\left(\frac{\bar{n}_e a^2}{\mu}\right)^{-1}.$$

Using the scaling (A2)-(A4) we can estimate the electron temperature, loop voltage and energy confinement time. As an example, for the CASTOR tokamak, supposing $\mu = 5\times10^{19}\,m^{-1}s^{-1}$:

$$T_e^0 = 88\left[\frac{I_p\sqrt{Z_{eff}}}{\Delta}\right]^{4/5} \qquad [eV,\ 10kA],$$

$$U_{loop} = 2\pi RE = 1.5\left[\frac{Z_{eff}^2}{I_p \Delta^4}\right]^{1/5} \quad [\text{V, 10kA}],$$

$$\tau_{Ee} = 1.5\, \bar{n}_e\, \tau_{Ee}^{Norm} \quad [\text{ms, } 10^{19}\text{m}^{-3}].$$

upposing $Z_{eff} = 2$, $\Delta = 0.8$ ($\beta < 0.5$), we obtain:

$$T_e^o = 138\left[I_p\right]^{4/5} \quad [\text{eV, 10kA}],$$

$$U_{loop} = 2.2\left[\frac{1}{I_p}\right]^{1/5} \quad [\text{V, 10kA}],$$

$$\tau_{Ee} = 0.45\, \bar{n}_e \quad [\text{ms, } 10^{19}\text{m}^{-3}].$$

hese dependences of T_e^o and U_{loop} predicted by such simple odel are compared with the experimental results in Fig. A4. t can be seen, that the dependence of the electron temperature n the center corresponds quite well to the experimentally letermined values. The agreement of the loop voltage with the xperiment, however, is only qualitative.

FERENCES

] Stöckel J. et al.: 7th Conf. of Czech. Physicists, Prague 1981

] CASTOR tokamak Group: IPPCZ-256, Prague, November 1985

] Andrjukhina E.D. et al.: Preprint No 217, Lebedev Physical Institute, Moscow 1982 (in russian)

] Korotkov A.A., Badalec J.: Res. Rept. ÚFP ČSAV No 9/85, Prague, December 1985 (in russian)

] Roberts D.E.: Nucl. Fus. 23(1983) 311-329

] Wesson J. et al.: 12th Europ. Conf. on Contr. Fus. and Plasma Phys., Proc. I, p. 147, Budapest 1985

] Murakami M.: Nucl. Fus. 16(1976) 347

] Kadomtsev B.B.: Plasma Phys. and Contr. Fus. 26(1984)1A, 217

] TFR Group: Rep. EUR-CEA-FC-883, 1977

] Carreras B. et al.: Nucl. Fus. 19(1979) 1423

] Djabilin K.S. et al.: Res. Rept. ÚFP ČSAV No 10/85, Prague, December 1985

ure captions:

1. Evolution of the low density discharge on CASTOR tokamak, B_T = 1.3 T.
2. Radiated and heating power P_{RAD} and P_{OH} versus average plasma density $\bar{n}_e$ for a few values of plasma current.
3. Calculated dependence of the total power P_{ei} transferred from electrons to ions on plasma density for CASTOR tokamak assuming $T_e(r) > 2T_i(r)$.
4. Power losses by electron thermal conductivity versus plasma current for low density discharges on CASTOR tokamak.
5. Power balance versus average density $\bar{n}_e$ for the three values of the plasma current (I_p= 7; 12; 17 kA, B_T= 1.3 T), low and medium density discharges.
6. Temporal evolution of the average electron density $\bar{n}_e$, radiative power losses P_{RAD} and relative intensity of the oxygen spectral line O VI (λ = 103 nm) at high density regime (I_p= 17 kA, B_T= 1.3 T).
7. Power balance versus average density $\bar{n}_e$ for the three values of plasma current (I_p= 12; 14; 17 kA), high density discharges.
8. Calculated width of the electron temperature radial profile Δ versus relative radiative power losses.
9. Temporal evolution of a high density discharge ($\bar{n}_e^{MAX}$ = = 4.5x10^{19} m^{-3}; I_p= 17 kA; B_T= 1.3 T) with a minor disruption at t = 5.7 ms.

Fig. 10. Hughill plot of density limit disruptions ($R = 0.4$ m, $B_T = 1.3$ T).

Fig. 11. Comparison of signal from four magnetic probes, uniformly distributed around the liner in a poloidal cross-section. Correlation of signals indicates an existence of the mode $m = 2$. Time „0" corresponds to a disruption.

Fig. 12. Temporal evolution of the ratio $\tilde{B}_\varphi/B_\varphi$, frequency of the oscillations for corresponding mode number f/m and the width of the magnetic island (for $m = 2$).

Fig. 13. Calculated resonant radius and island width for modes $m/n = 1/1;\ 2/1;\ 3/2$ versus parameter α of the model current distribution $j = j(0)(1 - r^2/a^2)^{\alpha}$.

Fig. A1. Equivalent circuit of the pyroelectric detector.

Fig. A2. Radial behaviour of the terms in eq. (A1'') in App. 2.

Fig. A3. Normalized energy confinement time versus relative radiated power (see eq. (A5)).

Fig. A4. Central electron temperature T_e^o and loop voltage U_{loop} versus plasma current; comparison of the experimental data with calculated scalings (A2) and (A3).

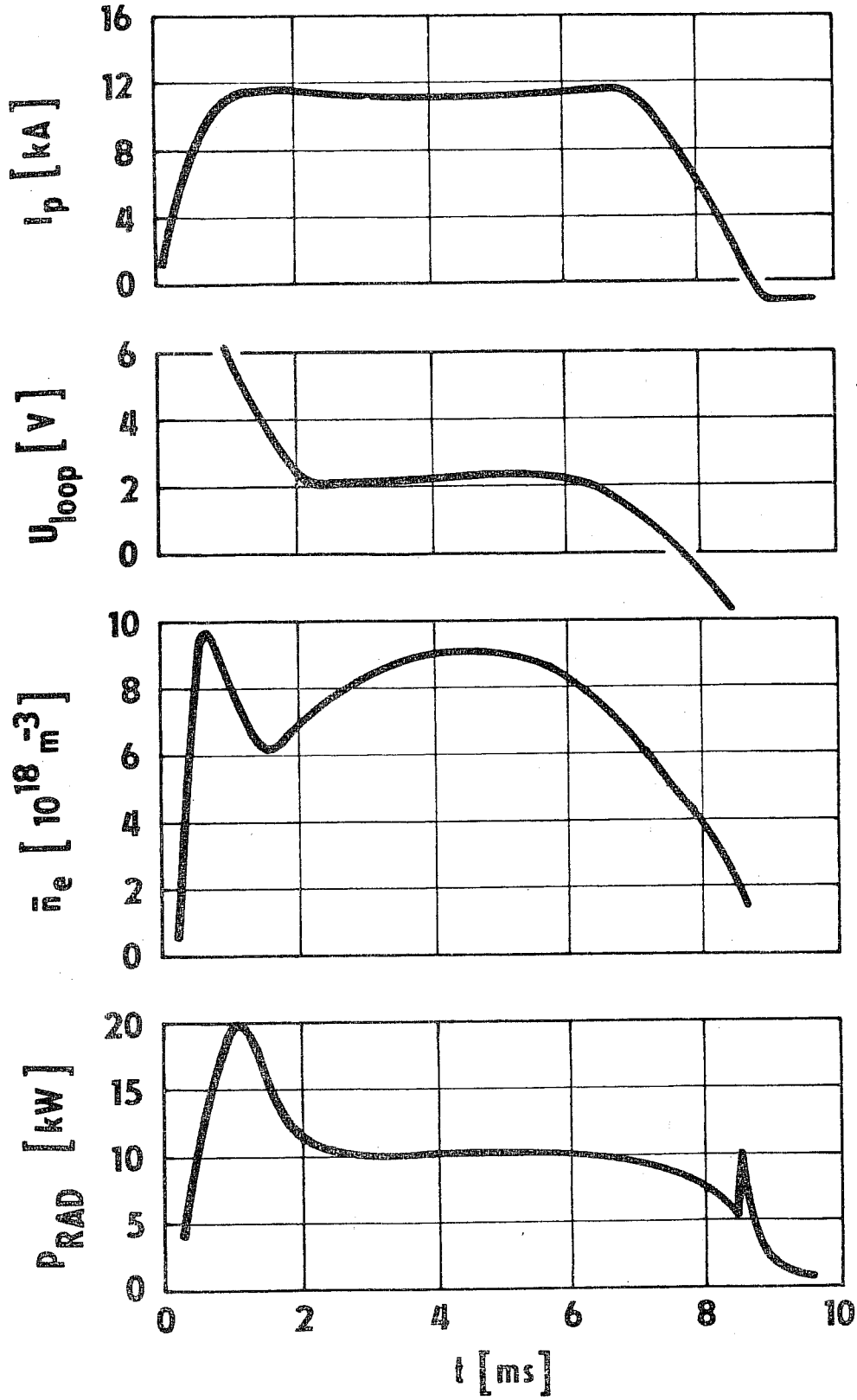
16
12
8
4
0
I_p [kA]
6
4
2
0
U_{loop} [V]
10
8
6
4
2
0
n_e [10^{18} m^{-3}]
20
15
10
5
0
P_{RAD} [kW]
0
2
4
6
8
10
t [ms]

FIG. 1

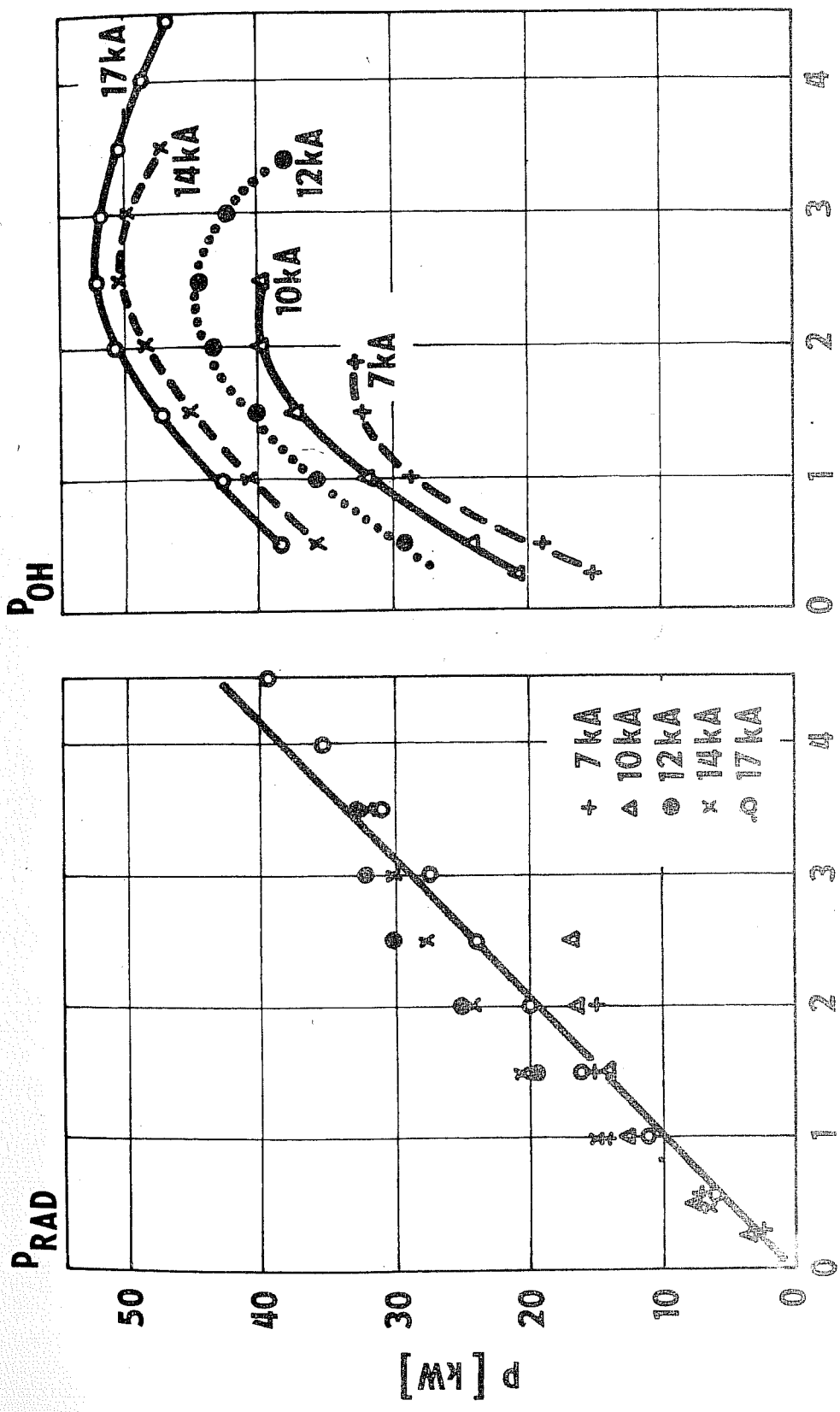
P [kW]
50
40
30
20
10
0
P_RAD
+ 7kA
Δ 10kA
● 12kA
× 14kA
○ 17kA
0
1
2
3
4
n_e [10^19 m^-3]
P_OH
17kA
14kA
12kA
10kA
7kA
0
1
2
3
4

FIG. 2

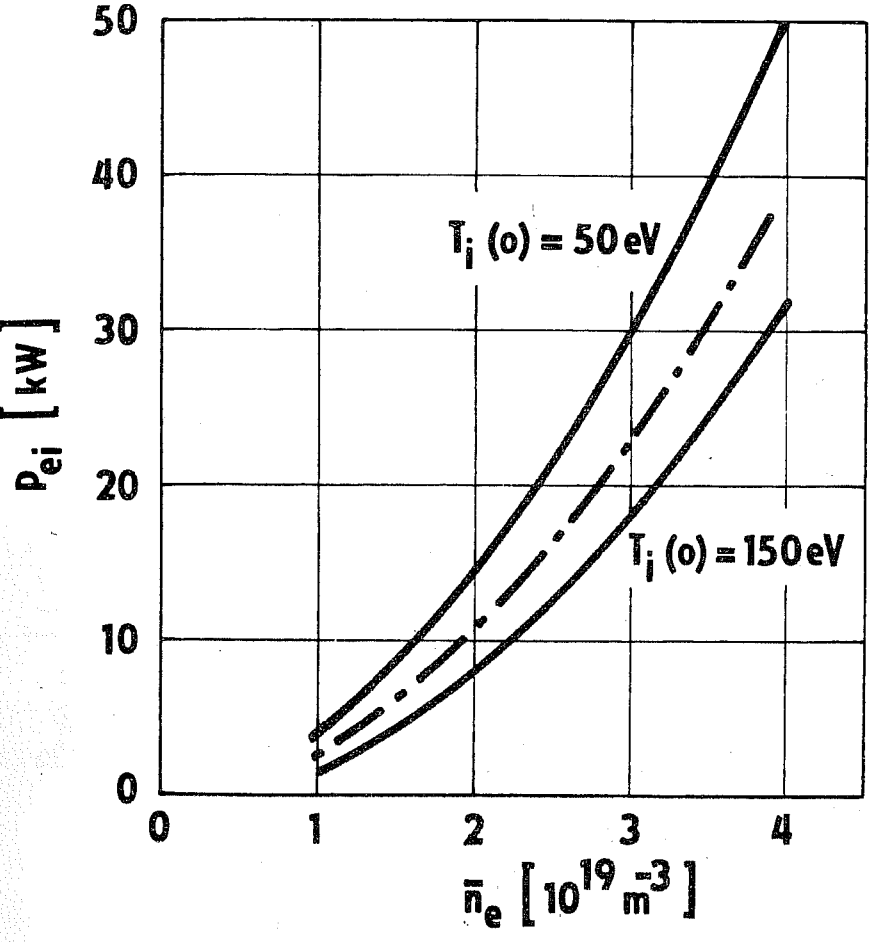

FIG. 3

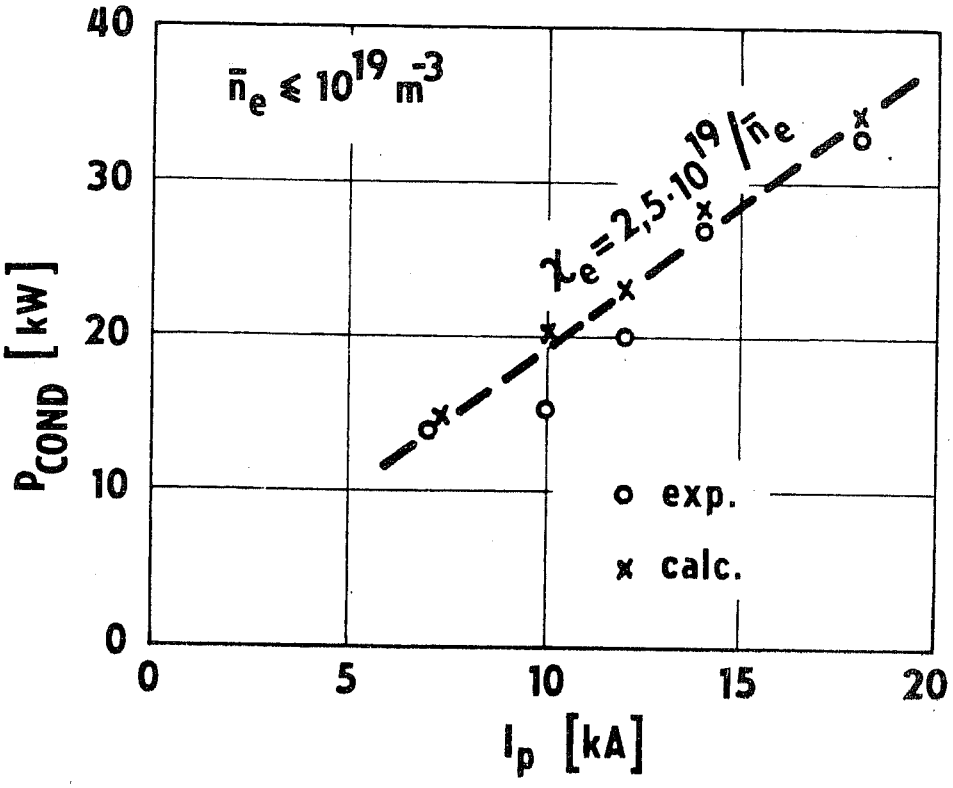
$\bar{n}_e \leq 10^{19}\ m^{-3}$
$\chi_e = 2{,}5 \cdot 10^{19} / \bar{n}_e$
o exp.
x calc.
P_{COND} [kW]
I_p [kA]
0
10
20
30
40
0
5
10
15
20

FIG. 4

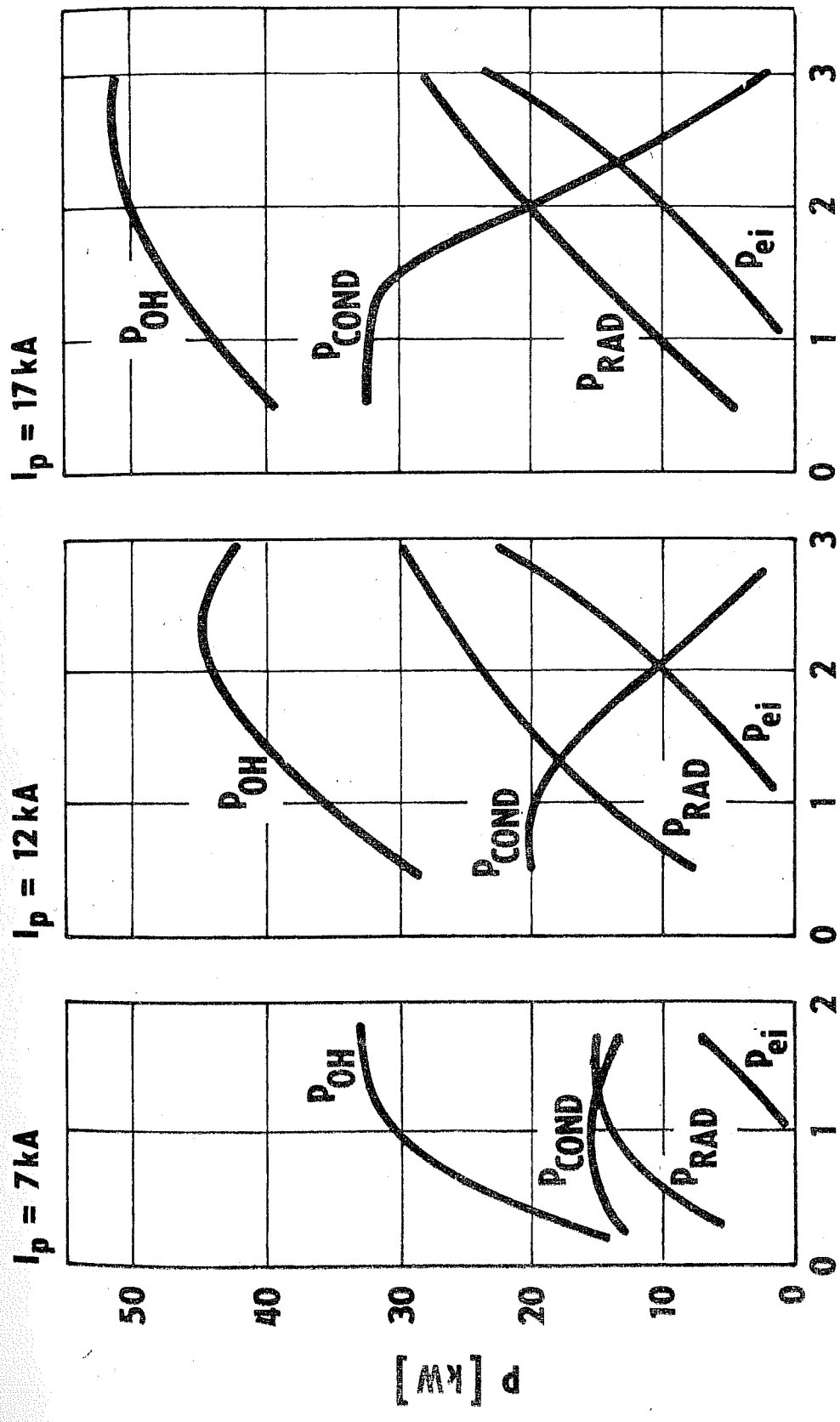
I_p = 7 kA
I_p = 12 kA
I_p = 17 kA
P_{OH}
P_{COND}
P_{RAD}
P_{ei}
P [kW]
50
40
30
20
10
0
0
1
2
3
$\bar{n}_e$ [10^{19} m^{-3}]

FIG. 5

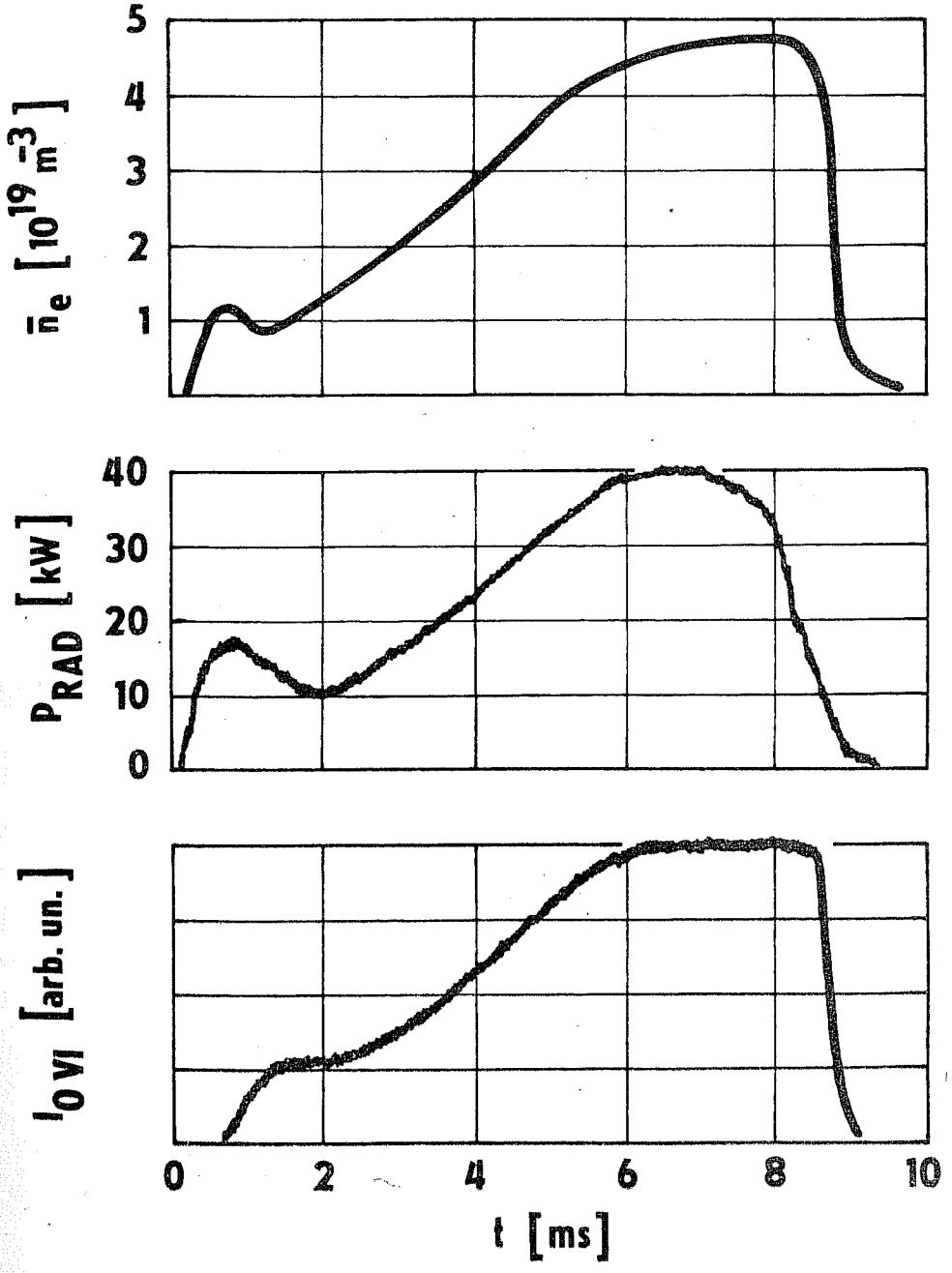
5
4
3
2
1
$\bar{n}_e$ [10^{19} m^{-3}]
40
30
20
10
0
P_{RAD} [kW]
I_{OVI} [arb. un.]
0
2
4
6
8
10
t [ms]

FIG. 6

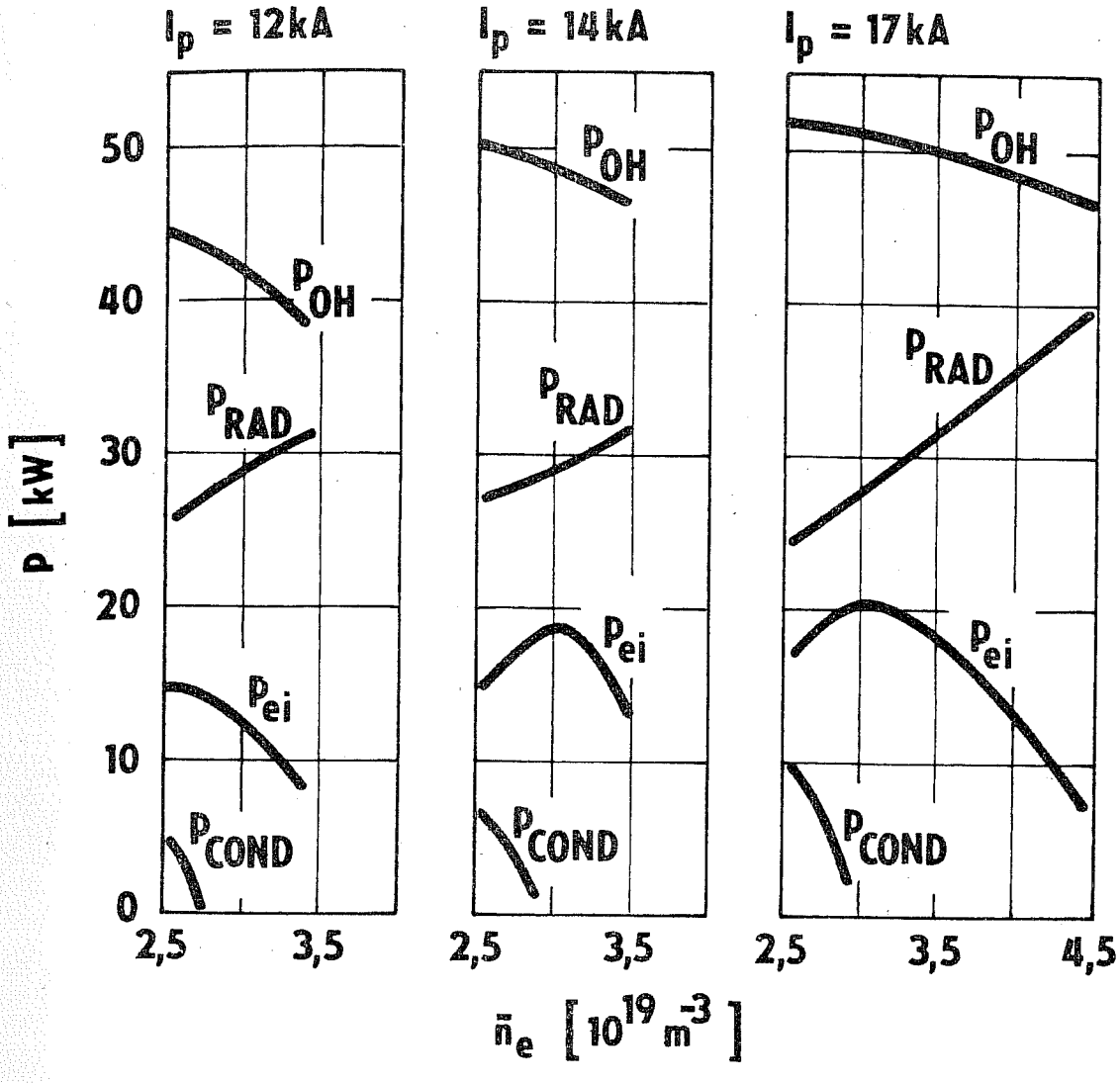
I_p = 12kA
I_p = 14kA
I_p = 17kA
P [kW]
50
40
30
20
10
0
P_{OH}
P_{RAD}
P_{ei}
P_{COND}
2,5
3,5
4,5
$\bar{n}_e$ [10^{19} m^{-3}]

FIG. 7

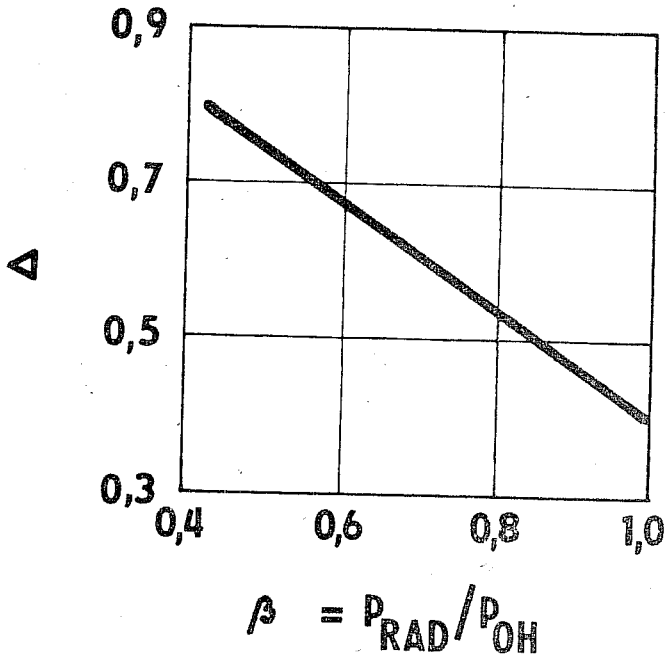

FIG. 8

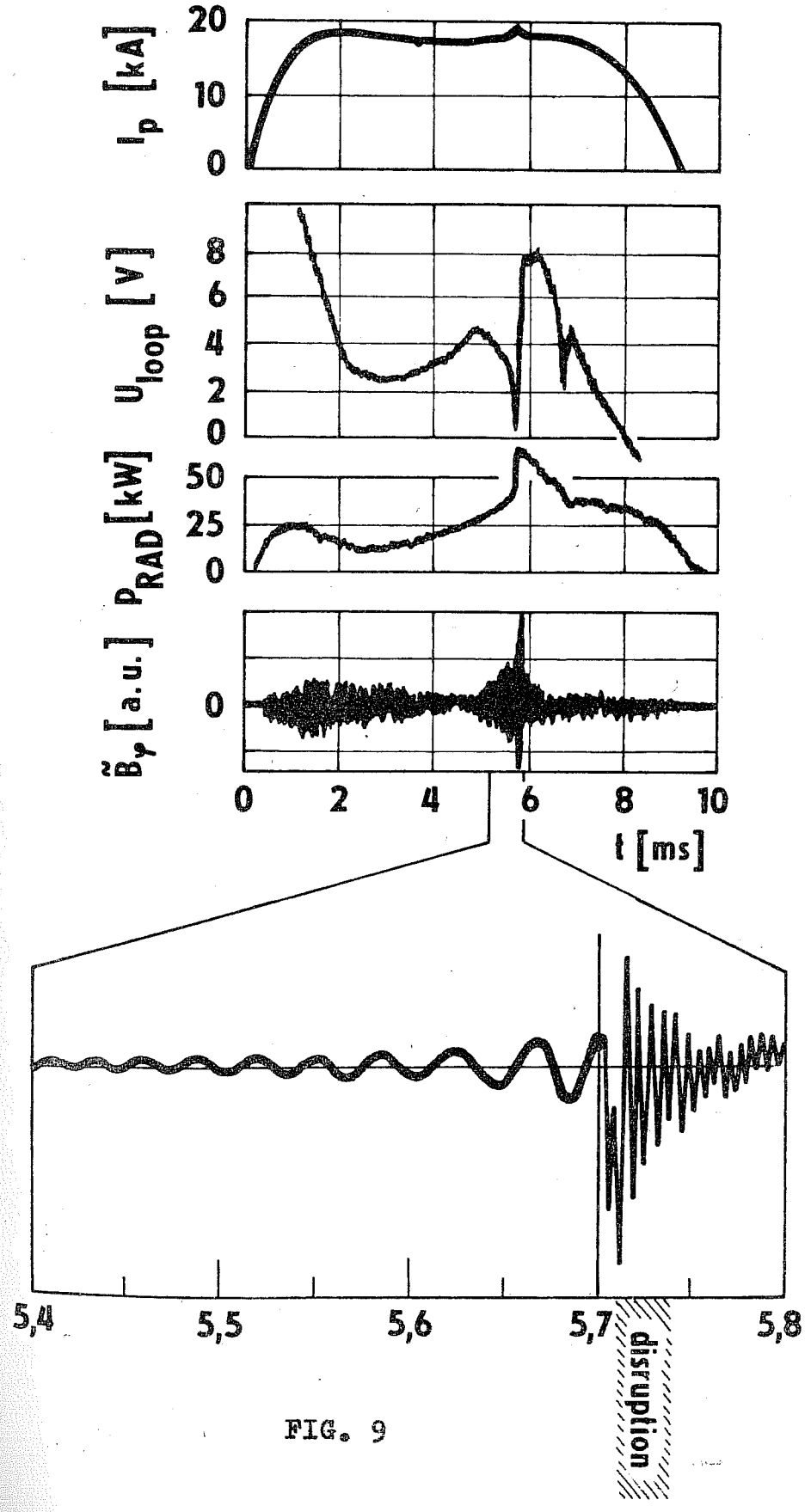
20
10
0
I_p [kA]
8
6
4
2
0
U_{loop} [V]
50
25
0
P_{RAD} [kW]
0
$\tilde{B}_\vartheta$ [a.u.]
0
2
4
6
8
10
t [ms]
5,4
5,5
5,6
5,7
5,8
disruption

FIG. 9

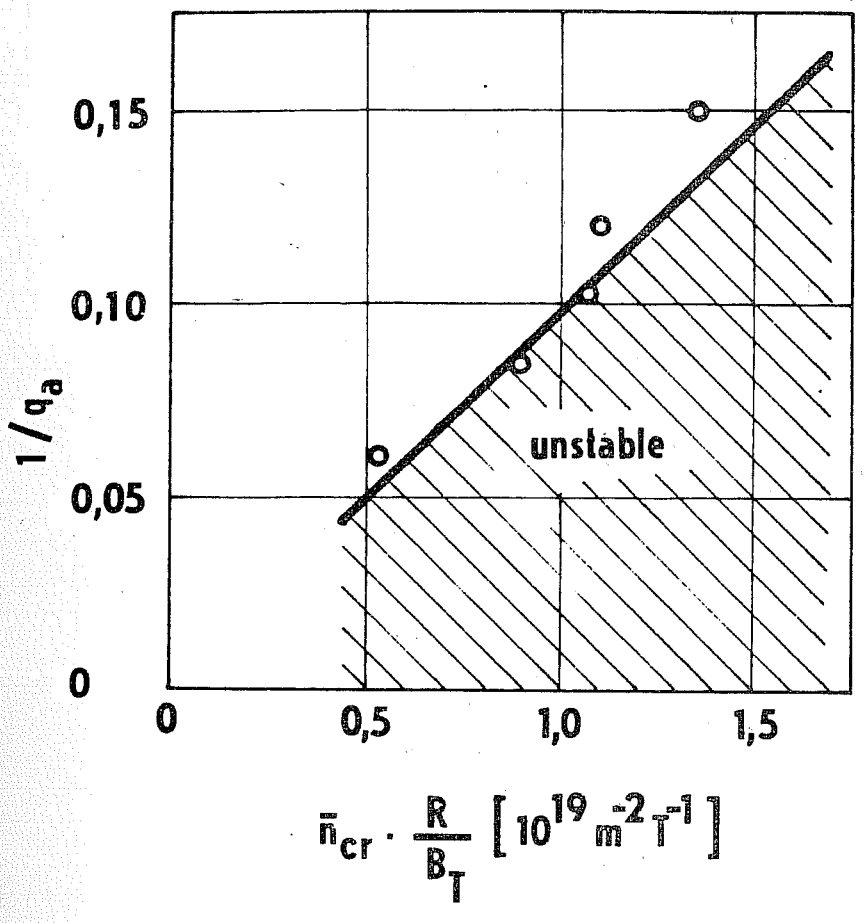

FIG. 10

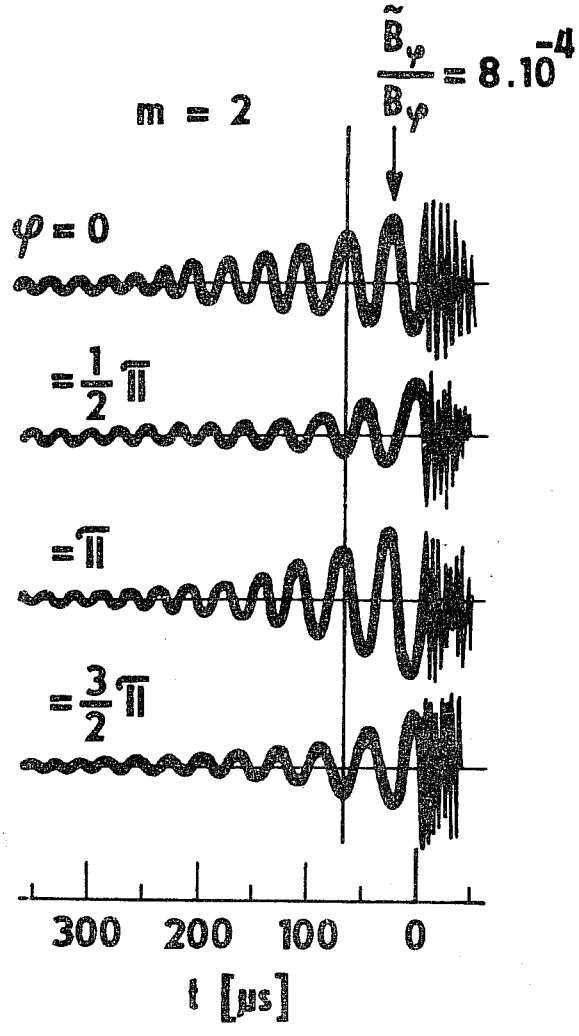
$\frac{\tilde{B}_\varphi}{B_\varphi} = 8.10^{-4}$
m = 2
$\varphi = 0$
$= \frac{1}{2}\pi$
$= \pi$
$= \frac{3}{2}\pi$
300
200
100
0
t [μs]

FIG. 11

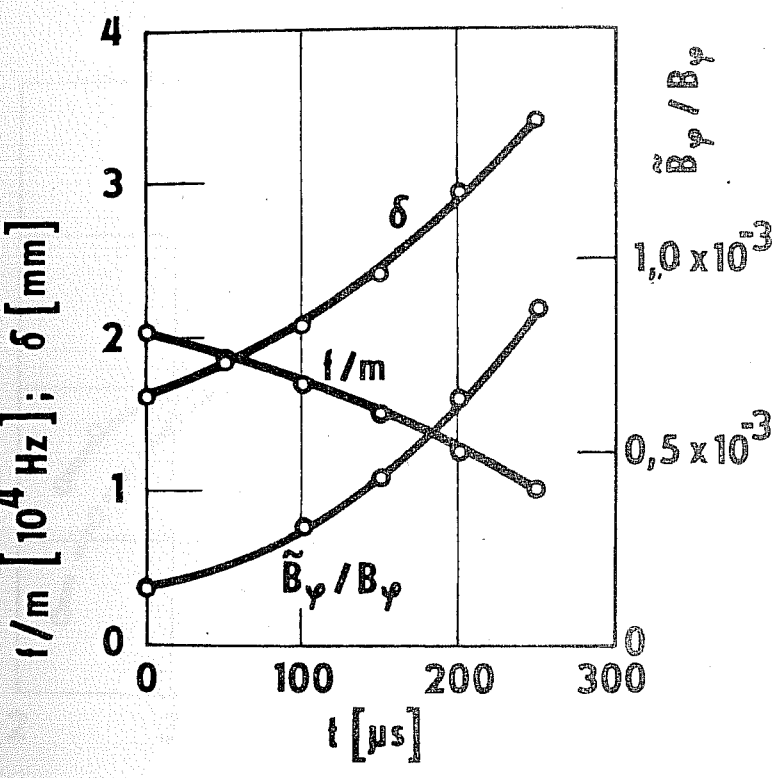

FIG. 12

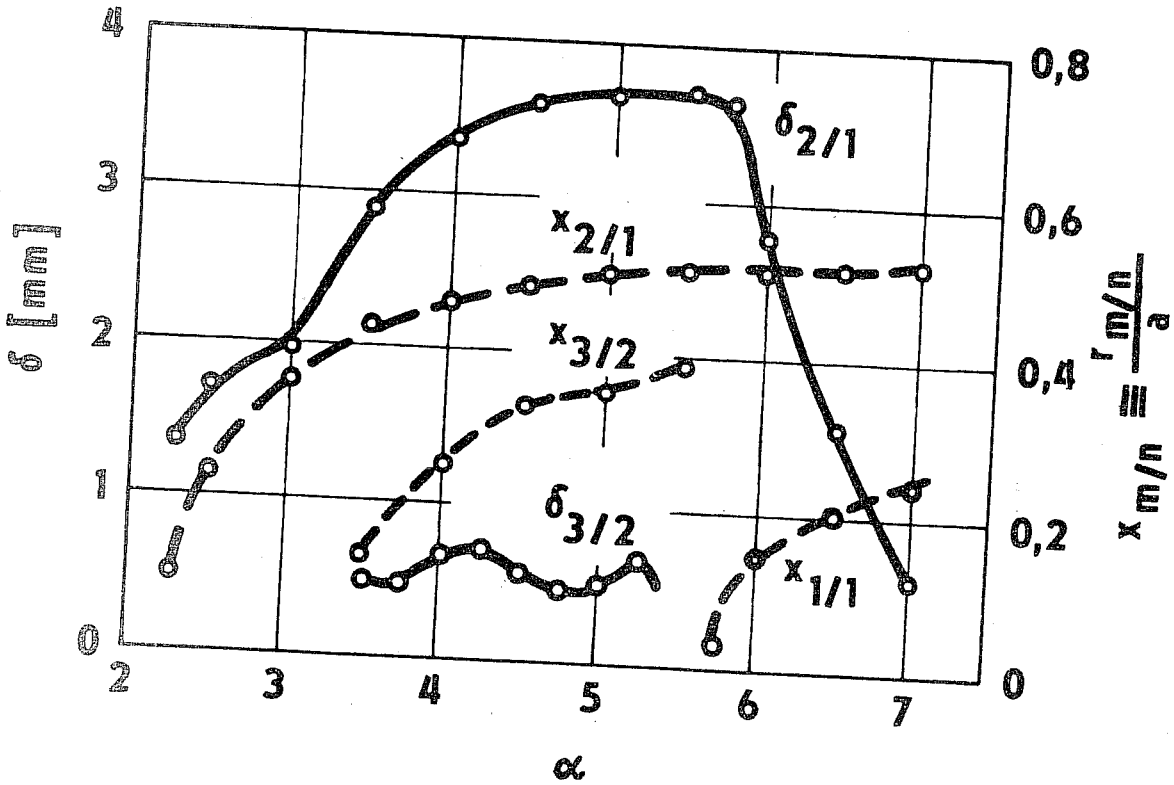
δ [mm]
$x_{m/n} \equiv \frac{r_{m/n}}{a}$
α
$\delta_{2/1}$
$x_{2/1}$
$x_{3/2}$
$\delta_{3/2}$
$x_{1/1}$
0
1
2
3
4
0
0,2
0,4
0,6
0,8
2
3
4
5
6
7

FIG. 13

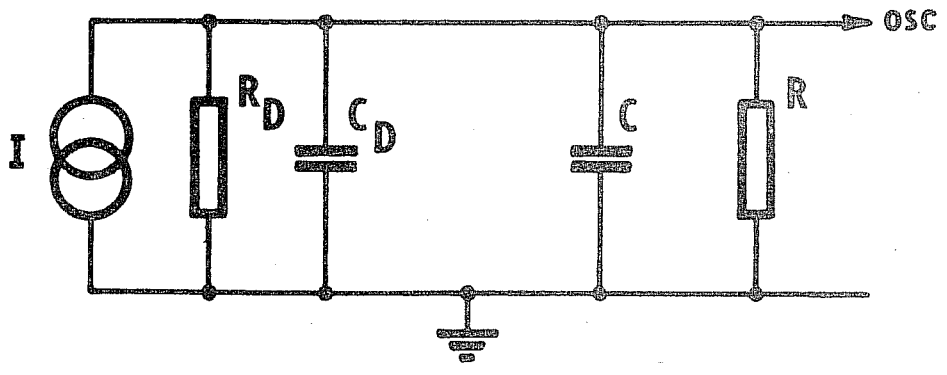

FIG. A1

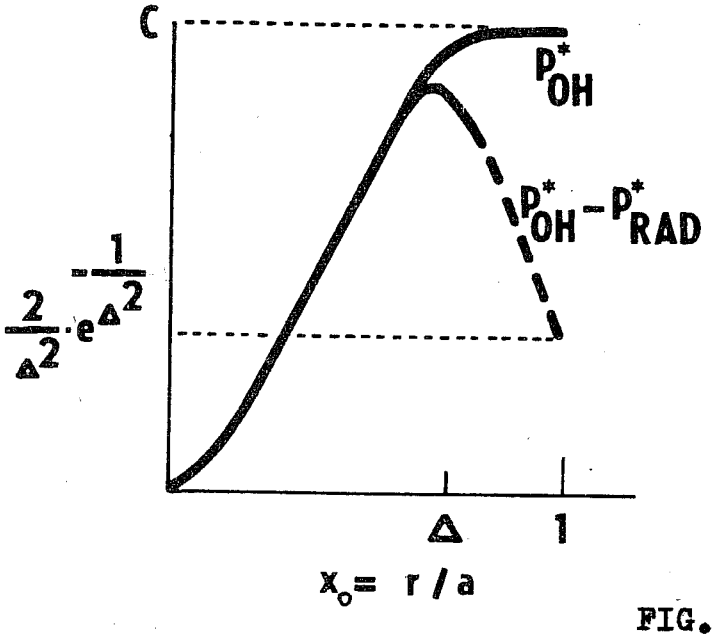
C
P^*_{OH}
$P^*_{OH} - P^*_{RAD}$
$\frac{2}{\Delta^2} \cdot e^{\Delta^2}$
$\frac{1}{}$
Δ
1
$x_o = r / a$

FIG. A2

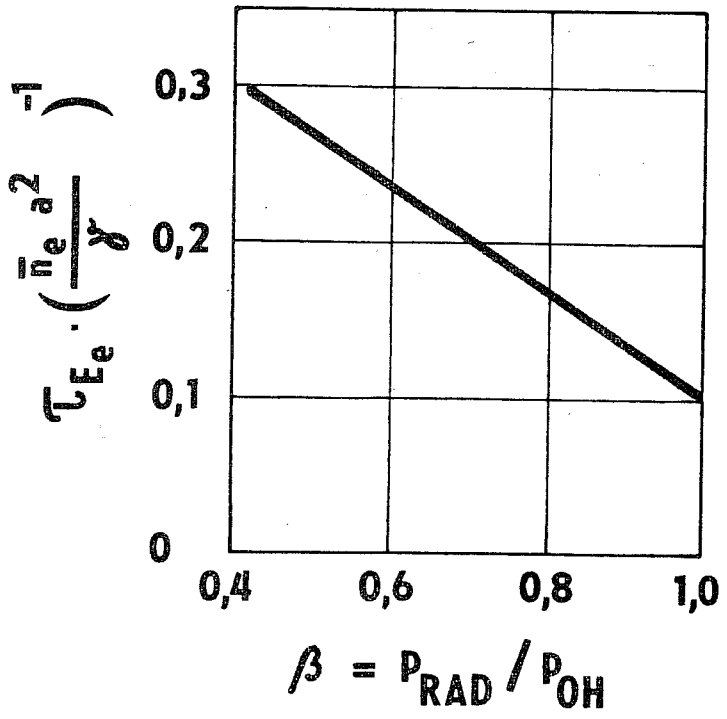
$\tau_{Ee} \cdot \left(\frac{\bar{n}_e a^2}{\gamma} \right)^{-1}$
0,3
0,2
0,1
0
0,4
0,6
0,8
1,0
$\beta = P_{RAD} / P_{OH}$

FIG. A3

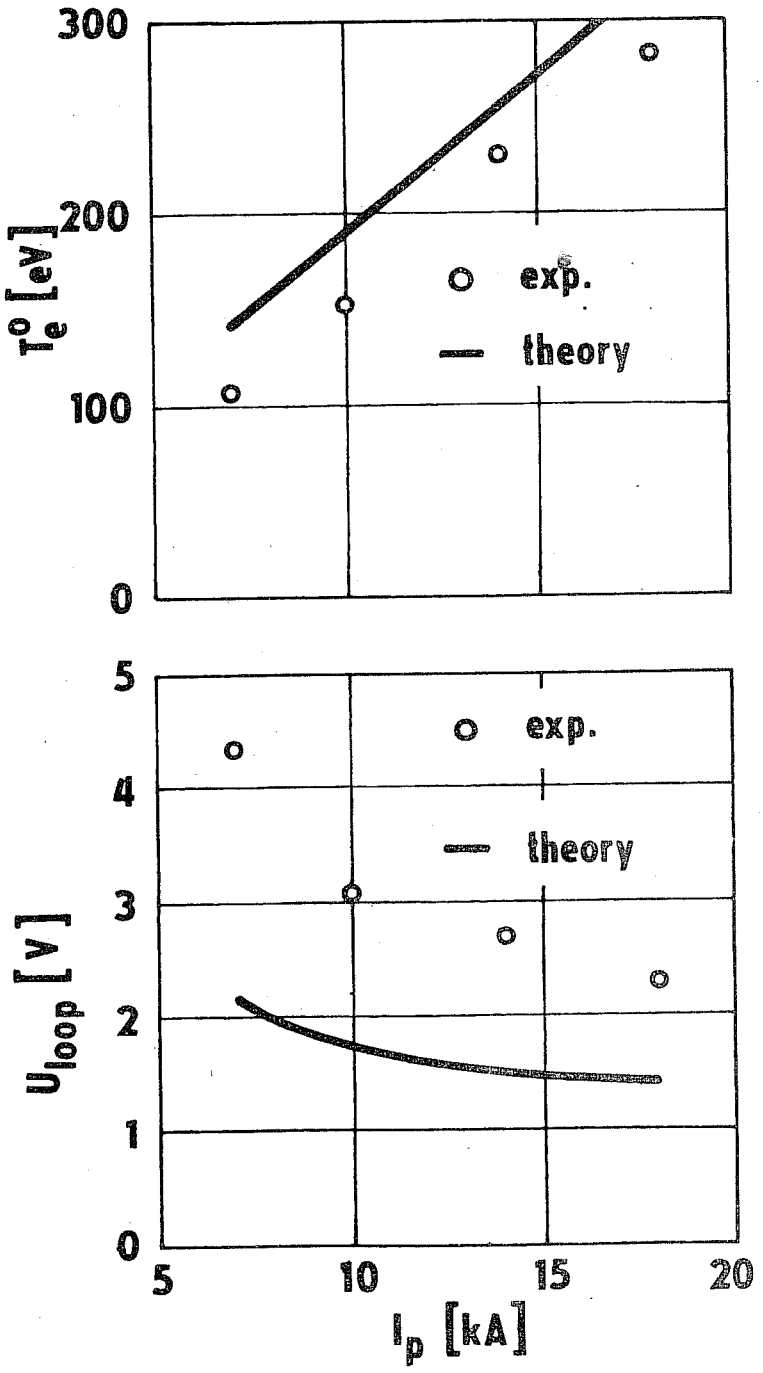
300
200
100
0
T_e^o [eV]
exp.
theory
5
4
3
2
1
0
U_{loop} [V]
exp.
theory
5
10
15
20
I_p [kA]

FIG. A4